Geomechanics and Engineering, *Vol. 28, No. 2 (2022) 197-207*
https://doi.org/10.12989/gae.2022.28.2.197

Seismic holding behaviors of inclined shallow plate anchor embedded in submerged coarse-grained soils

Nan Zhang[1,2], Hao Wang[3], Shuqi Ma*[4], Huaizhi Su[5] and Shaoyang Han[6]

[1]*School of Civil Engineering, Geotechnical and Structural Engineering Research Center, Shandong University, Jinan, Shandong 250061, PR China*
[2]*Department of Civil and Environmental Engineering, Colorado School of Mines, 1500 Illinois St., Golden, CO 80401, United States*
[3]*School of Civil and Construction Engineering, Oregon State University, 101 Kearney Hall, Corvallis, OR 97331, United States*
[4]*Key Laboratory of Transportation Tunnel Engineering, Ministry of Education, School of Civil Engineering, Southwest Jiaotong University, Chengdu, 610031, China*
[5]*State Key Laboratory of Hydrology-Water Resources and Hydraulic Engineering, Hohai University, Nanjing 210098, China*
[6]*Key Laboratory of Ministry of Education for Geomechanics and Embankment Engineering, Hohai University, Nanjing 210098, China*

(Received July 20, 2020, Revised December 18, 2021, Accepted December 20, 2021)

Abstract. The seismic holding behaviors of plate anchor embedded into submerged coarse-grained soils were investigated considering different anchor inclinations. The limit equilibrium method and the Pseudo-Dynamic Approach (PDA) were employed to calculate the inertia force of the soils within the failure rupture. In addition, assuming the permeability of coarse-grained soils was sufficiently large, the coefficient of hydrodynamic force applied on the inclined plate anchor is obtained through adopting the exact potential flow theory. Therefore, the seismic holding resistance was calculated as the combination of the inertia force and the hydrodynamic force within the failure rupture. The failure rupture can be developed due to the uplift loads, which was assumed to be an arc of a circle perpendicular to the anchor and inclines at ($\pi/4 - \varphi/2$). Then, the derived analytical solutions were evaluated by comparing the static breakout factor N_γ to the published experimental and analytical results. The influences of soil and wave properties on the plate anchor holding behavior are reported. Finally, the dynamic anchor holding coefficients $N_{\gamma d,}$ were reported to illustrate the anchor holding behaviors. Results show that the soil accelerations in x and z directions were both nonlinear. The amplifications of soil accelerations were more severe at lower normalized frequencies ($\omega H/V$) compared to higher normalized frequencies. The coefficient of hydrodynamic force, C, of the plate anchor was found to be almost constant with anchor inclinations. Finally, the seismic anchor holding coefficient oscillated with the oscillation of the inertia force on the plate anchor.

Keywords: inclined plate anchor; offshore anchors; pseudo-dynamic approach; seismic holding capacity; submerged soils

1. Introduction

In recent years, wave energy farms are built off the coastlines of major continents, such as pacific northwest of North America, Brazilian coastal. There are several kinds of wave energy converters (WECs) installed in the wave energy farms. The WECs are floating structures to generate electricity with high demands of offshore anchors to keep them in stations. The water depths of some of the testing farms are in excess of 150 m, so that the conventional offshore foundations (e.g., piles) could not perform these duties efficiently. Plate anchor is one of the commonly used anchor types for deep ocean applications (e.g., Randolph and Gourvenec 2011). Offshore plate anchors could be installed via pile or suction caisson (Randolph and Gourvenec 2011), which are initially vertically installed and then rotated to the place where perpendicular to the loads (sometime along with chains). The plate anchor will rotate till horizontal if the vertical loading is applied on the plate anchor. However, due to the moments applied on the plate anchor and the soil resistance, the plate anchor will not be rotated till the direction perpendicular to the loading, i.e., there are inclinations existing. According to the literature (O'Loughlin *et al*. 2006, 2012, Gaudin *et al*. 2008, Yu *et al.* 2009, Song *et al.* 2009, Bhattacharya and Sahoo 2017, Zhang *et al.* 2019), the anchor inclines ranging from 8◦ to 24◦ to the horizontal depending on the soil and loading properties. Moreover, some of the wave energy testing farms where the marine sediments are coarse-grained sandy soils. Therefore, a sufficient understanding of the holding behaviors of inclined plate anchor is significantly important not only for the current testing but for the future engineering practices.

The anchor holding capacities of plate anchor under static conditions have been studied by several researchers, (Meyerhof and Adams 1968, Rowe and Davis 1982, Murray and Geddes 1987, Dickin 1988, Merifield *et al.* 2003, Merifield and Sloan 2006, Kumar 2001, Zhang 2018, Bhattacharya 2017, Biradar *et al*. 2019, Evans and Zhang 2019) via experiments and numerical simulations. However, there are highly potentials and risks that the earthquake occurs in the subduction zones where some of the wave energy farms are located, e.g., west coast of U.S. and east

∗Corresponding author, Ph.D.
E-mail: shuqima.ma@gmail.com; shuqima@qq.com

ISSN: 2005-307X (Print), 2092-6219 (Online)

coast of Japan. The ocean floor motions will therefore influence the holding capacities of the embedded plate anchors. Seismic holding capacity of plate anchor was studied by several researchers (Kumar 2001, Choudhury and Subba Rao 2005, Ghosh 2009, 2010, Rangari *et al*. 2013, Pain *et al*. 2015). Among the above studies, the seismic holding capacities of plate anchor were obtained by using the pseudo-static approach (PSA) (Steedman and Zeng 1990, Rangari *et al*. 2013) and PDA, which were extended from pseudo-static approach introduced by Mononobe (1929) and Kumar (2001) and pseudo-dynamic approach presented by Ghosh (2009), respectively. PDA was first introduced to investigate the earth pressures on the retaining structures, where the soils are assumed to be dry and no hydrodynamic forces are induced. For a sinusoidal shaking, the accelerations are assumed to vary linearly in both vertical and horizontal directions. The accelerations at any depth below the mudline are expressed as Eqs. (1) and (2).

$$a_h(z,t)=\left[1+\frac{H-z}{H}\left(f_a-1\right)\right]a_h g\sin\left[\omega\left(t-\frac{H-z}{V_s}\right)\right] \quad (1)$$

$$a_v(z,t)=\left[1+\frac{H-z}{H}\left(f_a-1\right)\right]a_v g\sin\left[\omega\left(t-\frac{H-z}{V_p}\right)\right] \quad (2)$$

where a_h, a_v are horizontal and vertical earthquake acceleration coefficients, respectively, f_a is the amplification factor, V_s is the shear wave velocity, and V_p is the primary wave velocity. The inertia forces are calculated by integrating the product of mass and accelerations of the soil above the plate anchor with respect to the Newton's second law.

The PSA (Steedman and Zeng 1990) and PDA presented by Ghosh (2009) were applied to study the seismic holding capacities of horizontal plate anchors and inclined plate anchors. However, these approaches assumed the magnitudes and phases of accelerations in both *x* and *z*-directions were changing linearly with the embedment depth, which was different from the real scenario in the soil media. Based on the viscoelastic behaviors of the soils, Bellezza (2014) presented a modified PDA considering not only the material properties but the wave propagation behaviors in the soil media. The modified PDA was soon applied to the applications of several geostructures, e.g., retaining walls, plate anchors (Bellezza 2014, 2015, Pain *et al*. 2015, Chakraborty and Choudhury 2014). Nonetheless, offshore anchors were embedded into the submerged soils where the holding resistance should not only consider the influence of soil media but the hydrodynamic forces applied by water. Compared to the seismic thrust of retaining wall (Kumar 2001), the holding resistance of submerged plate anchor under seismic loading can be decomposed into three different parts: 1) the inertia forces applied on the anchor, 2) the hydrodynamic pressures on the plate anchor, and 3) the potential excess pore water pressures. Dynamic soil and water pressures of submerged soils can also be calculated considering the permeability and the geometry of the retaining soils by introducing a term called "restricted" water content (Matsuzawa *et al.* 1985). Contrary to "restricted", Matsuzawa *et al.* (1985) state that for highly permeable coarse-grained soil such as gravel and sand, most of the pore water belong to free water category.

In the previous studies, seismic holding behaviors of inclined plate anchor were introduced without considering the water conditions, and hydrodynamic forces on the emerged sloping structures were presented without considering soil effects. The seismic holding behaviors of the inclined plate anchor embedded into submerged coarse-grained soils have not been studied yet. In this paper, the combination of PDA and exact potential flow theory are used to calculate both the soil and hydrodynamic force applied on the inclined plate anchor. The inertia force of the soil was calculated by the latest-introduced PDA by Bellezza (2014). The seismic holding capacity of the plate anchor were calculated by adding the inertia force to the hydrodynamic forces applied on the plate anchor. The failure rupture of the inclined anchor was assumed as reported by Harvey and Burley (1973). Different from the previous studies (Rangari *et al.* 2013, Pain *et al*. 2015), in which imaginary retaining wall faces are assumed to illustrate the seismic behaviors, the paper consider the soil within the failure ruptures as a whole and obtain the dynamic holding coefficients to illustrate the seismic behaviors of inclined plate anchor embedded into submerged coarse-grained soils.

2. Methodology

2.1 Soil accelerations

For waves traveling in real materials, the energy loss will result in the decreases of the wave amplitudes. Viscous damping is used to represent the dissipation of the wave energy (Kramer 1996). Soils are assumed to be the viscoelastic media that the resistances to shearing deformation are the combination of both elastic part and viscous part. Kelvin-Voigt model shown in Fig. 1 is usually used to illustrate the soils (Hardin 1965), the stress-strain relation for a Kelvin-Voigt media is expressed as Eq. (3).

$$\tau=G\gamma+\eta\frac{\partial\gamma}{\partial t} \quad (3)$$

where τ is the shear stress, γ is the shear strain, and η is the viscosity of the soil. For a harmonic shear strain $\gamma=\gamma_0\sin\omega t$, the shear stress can be expressed, by substituting into Eqn. (3), as

$$t=G\gamma_0\sin\omega t+\omega\eta\gamma_0\cos\omega t \quad (4)$$

where γ_0 is the initial shear strain. As reported by Yuan *et al.* (2016), Bellezza (2014), and Rajesh and Choudhury (2017), the one dimensional equation of motion for waves propagating in the Kelvin-Viogt medium is expressed as Eq. (5)

$$\rho\frac{\partial^2 u}{dt^2}=\left[\left(\lambda+G\right)+\left(\eta_1+\eta_2\right)\frac{\partial}{\partial t}\right]grad\left(\overline{\Theta}\right)+\left(G+\eta_2\frac{\partial}{\partial t}\right)\nabla^2 u \quad (5)$$

where ρ is the soil density, η_1 and η_2 are viscosities of the

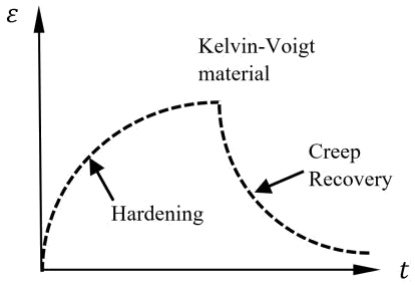

Fig. 1 Kelvin-Voigt material

soil, λ is the Lamé's first parameter, G is shear modulus, Θ = div(**u**), u is the displacement vector.

The equation of motion of a wave vertically propagating through the Kelvin-Voigt media can be expressed as Eqs. (6) and (7) as:

$$\rho\frac{\partial^2 u}{dt^2}=G\frac{\partial u_x^2}{dz^2}+\eta_2\frac{\partial^3 u_x}{\partial z^2\partial t} \tag{6}$$

$$\rho\frac{\partial^2 u}{dt^2}=(\lambda+2G)\frac{\partial u_x^2}{dz^2}+(\eta_1+2\eta_2)\frac{\partial^3 u_x}{\partial z^2\partial t} \tag{7}$$

For a harmonic horizontal shaking, the solution of Eqn. 6 as reported by Bellezza (2014) as a function of damping ratio $\zeta_s = \eta_2\omega_s/(2G)$ and the normalized shear wave frequency $\omega_s H/V_s$. The displacement at ground surface is assumed to be zero, the displacement at the base of the plate anchor is assumed to be $u_{bx} = u_{x0}\cos(\omega_s t)$. The displacement in x-direction within a layer of $z = H$ is given as Eq. (8).

$$u_x(z,t)=\frac{u_{x0}}{C_S^2+S_S^2}\begin{bmatrix}(C_SC_{sz}+S_SS_{sz})\cos(\omega_s t)\\+(C_SC_{sz}-S_SS_{sz})\sin(\omega_s t)\end{bmatrix} \tag{8}$$

The acceleration is the second derivative of the displacement as $a_{x0} = -\omega_s u_{x0}$. The soil acceleration in x-direction is obtained from Eq. (8) as Eq. (9).

$$a_x(z,t)=\frac{a_{x0}}{C_S^2+S_S^2}\begin{bmatrix}(C_SC_{sz}+S_SS_{sz})\cos(\omega_s t)\\+(C_SC_{sz}-S_SS_{sz})\sin(\omega_s t)\end{bmatrix} \tag{9}$$

Where

$$C_{sz}=\cos\left(\frac{Y_{s1}z}{H}\right)\cosh\left(\frac{Y_{s2}z}{H}\right) \tag{10}$$

$$S_{sz}=-\sin\left(\frac{Y_{s1}z}{H}\right)\sinh\left(\frac{Y_{s2}z}{H}\right) \tag{11}$$

$$C_S=\cos(Y_{s1})\cosh(Y_{s2}) \tag{12}$$

$$S_S=-\sin(Y_{s1})\sinh(Y_{s2}) \tag{13}$$

$$Y_{s1}=\frac{\omega_s H}{v_s}\sqrt{\frac{\sqrt{1+4\zeta_s^2}+1}{2(1+4\zeta_s^2)}} \tag{14}$$

$$Y_{s2}=-\frac{\omega_s H}{v_s}\sqrt{\frac{\sqrt{1+4\zeta_s^2}-1}{2(1+4\zeta_s^2)}} \tag{15}$$

where ζ_s is the damping ratio of S-wave, C_{sz}, S_{sz}, C_S, S_S, Y_{s1}, and Y_{s2} are the factors governing the displacement and acceleration in x-direction.

For a harmonic shaking in vertical directions, the solution of Eq. (7) is shown in Eq. (16).

$$u_z(z,t)=\frac{u_{z0}}{C_P^2+S_P^2}\begin{bmatrix}(C_PC_{pz}+S_PS_{pz})\cos(\omega_p t)\\+(C_PC_{pz}-S_PS_{pz})\sin(\omega_p t)\end{bmatrix} \tag{16}$$

The vertical acceleration is given as Eqn. (17) by defining a_{z0}

$$a_z(z,t)=\frac{a_{z0}}{C_P^2+S_P^2}\begin{bmatrix}(C_PC_{pz}+S_PS_{pz})\cos(\omega_p t)\\+(C_PC_{pz}-S_PS_{pz})\sin(\omega_p t)\end{bmatrix} \tag{17}$$

Where

$$C_{pz}=\cos\left(\frac{Y_{p1}z}{H}\right)\cosh\left(\frac{Y_{p2}z}{H}\right) \tag{18}$$

$$S_{pz}=-\sin\left(\frac{Y_{p1}z}{H}\right)\sinh\left(\frac{Y_{p2}z}{H}\right) \tag{19}$$

$$C_P=\cos(Y_{p1})\cosh(Y_{p2}) \tag{20}$$

$$S_P=-\sin(Y_{p1})\sinh(Y_{p2}) \tag{21}$$

$$Y_{p1}=\frac{\omega_p H}{v_p}\sqrt{\frac{\sqrt{1+4\zeta_p^2}+1}{2(1+4\zeta_p^2)}} \tag{22}$$

$$Y_{p1}=-\frac{\omega_p H}{v_p}\sqrt{\frac{\sqrt{1+4\zeta_p^2}-1}{2(1+4\zeta_p^2)}} \tag{23}$$

where ζ_p is the damping ratio of P-wave, C_{pz}, S_{pz}, C_P , S_P, Y_{p1}, and Y_{p2} are the factors governing the displacement and acceleration in z-direction. The detailed derivation of the accelerations of Kelvin-Viogt material is reported by Bellezza (2014).

2.2 Inertia forces

Experimental and numerical studies indicate that for embedded plate anchors, there are certain rapture surfaces. Among them, Ilamparuthi and Muthukrishnaiah (1999), Liu *et al.* (2011), and Dyson and Rognon (2014) assume the rapture surfaces are planar. However, the rapture is not strictly planar as reported by Hu *et al.* (2021) and Liang *et al.* (2021). By referring to the published work in the literature and the principles of earth pressures for retention structures, in static conditions, the rupture surface of the

inclined plate anchor was assumed to be two circular arcs perpendicular to the lower edge of the plate anchor and with the tangential angle of $\theta_1=\theta_2=\pi/4-\varphi/2$ to the horizontal at the mudline, where φ is the soil internal friction angle, see Fig. 2. The calculation will be performed in $x_0 - z_0$ space, where the plate anchor is in x_0 direction and perpendicular to the z_0 direction. The soil mass of the wedge can be calculated at both negative and positive x_0 axes, respectively. R_L and R_R are the forces acting on left and right rapture, respectively.

The mass of the soil wedge in $+x_0$ direction can be calculated by subtracting the mass of CDE from OBCD. The mass of a thin element of the wedge is calculated by Eqs. (24) and (25).

$$m(z')_{OBCD}=\frac{\gamma_{sub}}{g}\left(\frac{L}{2}+R_R-\sqrt{(R_R)^2-z'^2}\right)dz' \tag{24}$$

$$m(z')_{CDE}=\frac{\gamma_{sub}}{g}\left[\begin{array}{l}\dfrac{z'}{\tan(\alpha)}-\dfrac{H\sin(\Gamma)}{\tan(\alpha)\sin(\Pi)}\\ +\dfrac{L}{2}+\dfrac{H\cos(\Gamma)}{\sin(\Pi)}\end{array}\right]dz' \tag{25}$$

where γ_{sub} is the buoyant unit weight of the soil, $\Gamma=\pi/4+\theta/2+\alpha/2$, and $\Pi=\pi/4+\theta/2-\alpha/2$. H_{OD} is calculated as Eq. (26).

$$H_{OD}=\frac{H\sin(\Gamma)}{\sin(\Pi)} \tag{26}$$

where H is the embedment depth of the lower edge of the plate anchor, α is anchor inclination. The radius of the right rupture surface, R_R, is calculated as Eq. (27).

$$R_R=\frac{H}{2\cos(\Gamma)\sin(\Pi)} \tag{27}$$

By substituting Eqs. (9) and (17) into Eqs. (24) and (25) and integrating in the corresponding domain, the inertial force of soil of the right wedge in z_0 direction is calculated as Eq. (28).

$$\begin{aligned}Q_{u+}=&\int_0^{H_{OD}}\frac{\gamma_{sub}}{g}\left(\frac{L}{2}+R_R-\sqrt{(R_R)^2-z'^2}\right)a_x(z,t)\sin(\alpha)dz'\\&+\int_0^{H_{OD}}\frac{\gamma_{sub}}{g}\left(\frac{L}{2}+R_R-\sqrt{(R_R)^2-z'^2}\right)a_z(z,t)\cos(\alpha)dz'\\&-\int_{H_{OE}}^{H_{OD}}\frac{\gamma_{sub}}{g}\left[\frac{z'-H_{OE}}{\tan(\alpha)}\right]a_x(z,t)\sin(\alpha)dz'\\&-\int_{H_{OE}}^{H_{OD}}\frac{\gamma_{sub}}{g}\left[\frac{z'-H_{OE}}{\tan(\alpha)}\right]a_z(z,t)\cos(\alpha)dz'\end{aligned} \tag{28}$$

Where,

$$H_{OE}=\frac{H\sin(\Gamma)}{\sin(\Pi)}-\left(\frac{L}{2}-\frac{H\sin(\Gamma)}{\sin(\Pi)\tan(\Gamma)}\right)\tan(\alpha) \tag{29}$$

The mass of the soil wedge in $-x_0$ direction can be calculated by adding the mass of EFG to OGFA. The mass of thin element of the wedge are calculated by Eqs. (30) and (31).

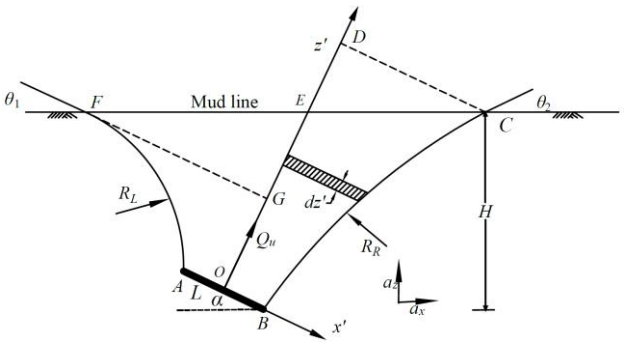

Fig. 2.Diagram of rupture surface of inclined plate anchor

$$m(z')_{OGFA}=\frac{\gamma_{sub}}{g}\left(R_L\cos(\alpha)+\frac{L}{2}+\sqrt{R_L^2-\left(z'+R_L\sin^2(\alpha)\right)}\right)dz' \tag{30}$$

$$m(z')_{EFG}=\frac{\gamma_{sub}}{g}\left[-\frac{z'-H_{OE}}{\tan(\alpha)}\right]dz' \tag{31}$$

where R_L is the radius of left failure rupture arc that can be calculated the by Eq. (32)

$$R_L=\frac{H-L\sin(\alpha)}{\sin(\pi/2-\theta)} \tag{32}$$

By substituting Eqs. (9) and (17) into Eqs. (30) and (31) and integrating in the corresponding domain, the inertial force of soil of the right wedge in z_0 direction is calculated as Eq. (33).

$$\begin{aligned}Q_{u-}=&\int_0^{H_{OG}}\frac{\gamma_{sub}}{g}\Omega\times a_x(z,t)\sin(\alpha)dz'\\&+\int_0^{H_{OG}}\frac{\gamma_{sub}}{g}\Omega\times a_z(z,t)\cos(\alpha)dz'\\&+\int_{H_{OG}}^{H_{OE}}\frac{\gamma_{sub}}{g}\left[\frac{H_{OE}-z'}{\tan(\alpha)}\right]a_x(z,t)\sin(\alpha)dz'\\&+\int_{H_{OG}}^{H_{OE}}\frac{\gamma_{sub}}{g}\left[\frac{H_{OE}-z'}{\tan(\alpha)}\right]a_z(z,t)\cos(\alpha)dz'\end{aligned} \tag{33}$$

Where

$$H_{OG}=R_L-R_L/\left[\left(\frac{1}{\tan(\pi/2-\theta)}+\frac{1}{\tan(\alpha)}\right)\sin\left(\frac{\pi}{2}-\theta\right)\right] \tag{34}$$

$$\begin{aligned}\Omega=&R_L\cos(\alpha)+\frac{L}{2}\\&-\sqrt{R_L^2-\left(z'+\frac{R_L\cos(\theta-\alpha)}{\left(\frac{1}{\tan(\pi/2-\theta)}+\frac{1}{\tan(\alpha)}\right)\sin\left(\frac{\pi}{2}-\theta\right)}\right)^2}\end{aligned} \tag{35}$$

The inertial force applied on the plate anchor in z_0-direction resulting from the soils are the summation of inertial force calculated from Eqs. (28) and (33) as Eq. (36).

$$Q_u=Q_{u+}+Q_{u-} \tag{36}$$

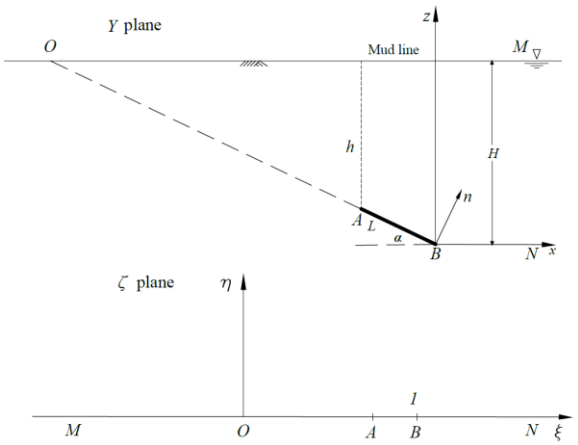

Fig. 3 The water in the physical *z* plane is conformally mapped into the upper half of the ζ plane

2.3 Effects of water on the plate anchor

The presence of water above the plate anchor plays a significant role in determining the holding forces of the plate anchor during earthquakes. Water flow downward relative to the anchor will exert dynamic pressures on the plate anchor. Inclined plate anchor has the similarity with retaining structures. For the submerged plate anchor, the water pressure is divided into two separate components, the hydrostatic pressure and hydrodynamic (Kramer 1996). The hydrodynamic forces of the inclined plate anchor in submerged soils can be calculated from the comparable calculations for hydrodynamic pressures on sloping dams during earthquakes (Chwang 1978a, b).

Based on the exact potential flow theory put forward by Chwang (1978a), Fig. 3 shows the conformal mapping of the water from physical Y plane to the upper half of the ζ plane, where $\zeta=\xi+i\eta$. The points O and B are mapped into ζ plane as $\xi=0$ and +1, where O is the virtual point of extension cord of the inclined plate anchor. The point A is mapped into ζ plane as $\xi_A=1-L\sin\alpha/H$. The total normal force on the inclined plate anchor as

$$F_n=\frac{H}{\pi}\int_{\xi_A}^{1}\left(\frac{\xi}{1-\xi}\right)^{\frac{\alpha}{\pi}}\frac{p(\xi)}{\xi}d\xi \tag{37}$$

Where

$$p(\xi)=\rho_w a_0 H\left[\frac{4}{\pi^2}\int_0^{\frac{\pi}{2}}\left(\frac{\xi}{\xi+\tan^2\alpha}\right)^{\frac{\alpha}{\pi}}\frac{\alpha d\alpha}{\sin\alpha\cos\alpha}-\cot\alpha+\frac{\cos\alpha}{H}s(\xi)\right] \tag{38}$$

$(\xi_A<\xi<1)$

where a_0 is the acceleration value at the middle of the plate anchor

$$s(\xi)=\frac{H}{\pi}\int_{\xi}^{1}\left(\frac{t}{1-t}\right)^{\frac{\alpha}{\pi}}\frac{dt}{t}\quad(\xi_A<\xi<1) \tag{39}$$

Eq. (37) can be reduced as

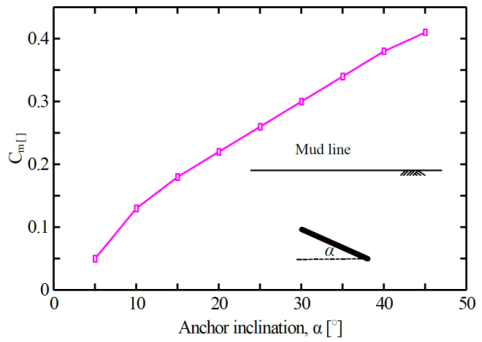

Fig. 4 Maximum coefficient of dynamic water pressure on the inclined structure

$$F_n=C_n\rho_w a_0(H^2-h^2) \tag{40}$$

where C_n is the normal force coefficient as

$$C_n=\frac{4}{\pi^2}\int_{\xi_A}^{1}\left(\frac{\xi}{1-\xi}\right)^{\frac{\alpha}{\pi}}\frac{d\xi}{\xi}\int_0^{\frac{\pi}{2}}\left(\frac{\xi}{\xi+\tan^2\alpha}\right)^{\frac{\alpha}{\pi}}\frac{\alpha d\alpha}{\sin\alpha\cos\alpha}-\frac{1}{2}\frac{\cos\alpha}{\sin^2\alpha} \tag{41}$$

Hydrodynamic water pressure results from the dynamic response of the body of water. For the inclined anchor embedded into submerged soils, the hydrodynamic force is able to be calculated based on the exact two-dimensional potential-flow theory by Chwang (1978a), where was used to calculate the hydrodynamic force on the rigid dam with inclined slope. The pressure coefficient result from horizontal acceleration can be calculated as Eq. (42).

$$C_p=\frac{F_n L}{\rho_w a_h h} \tag{42}$$

Hydrodynamic pressure coefficient result from horizontal acceleration can also be calculated by Chwang (1978b) as

$$C_p=\frac{C_m}{2}\left[\frac{h}{H}\left(2-\frac{h}{H}+\sqrt{\frac{h}{H}\left(2-\frac{h}{H}\right)}\right)\right] \tag{43}$$

where C_m is the maximum value of C_p, the relationship between C_m and anchor inclinationangle is presented by Zangar (1953), which shown in Fig. 4.

According to Figs. (3) and (4), the hydrodynamic pressure coefficients at different anchor inclinations was only applied on the depths ranging from ξ_A to 1, where ξ_A corresponds to the upper edge of the plate anchor, where the depth is $h=H-L\sin\alpha$, and 1 corresponds to the bottom edge of the anchor, where the depth is H. The hydrodynamic pressure coefficients are shown in Fig. 5.

The embedded plate anchor is assumed to be rigid, which means that the normal velocity (in *n* direction in Fig. 3) of the water adjacent to the plate anchor should be the same as the velocity of the plate anchor Chwang (1978b). The location of plate anchor keeps relatively static. Thus the acceleration in front of the plate anchor is constant. Fig. 5

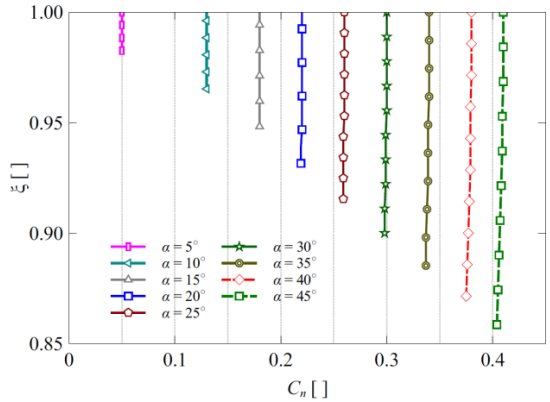

Fig. 5 The hydrodynamic pressure coefficients of anchor plate for different inclinations

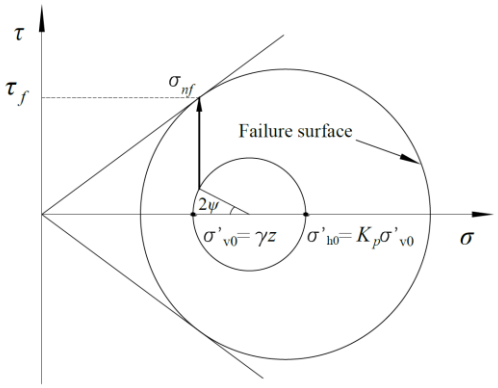

Fig. 6 Assumed Mohr's circles

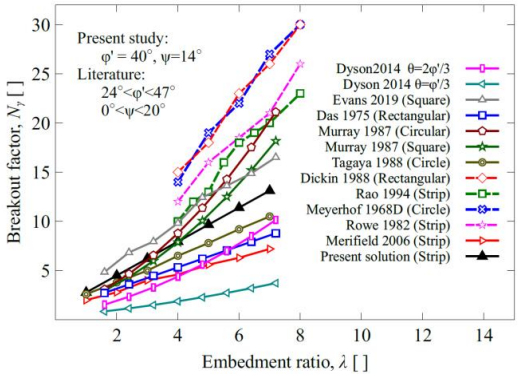

Fig. 7 Comparisons between the present solution (α=0°) and published results in the literature (after Evans and Zhang 2019)

shows the hydrodynamic pressure coefficient along the depth for different anchor inclination. In the analysis, the acceleration is selected as the average value of the hydrodynamic pressure coefficients along the plate anchor.

3. Results and discussion

3.1 Comparison to published experimental results

Since there is no published experimental work about seismic holding capacity of inclined plate anchor embedded into submerged soils, the evaluation of the analytical solution in this work is based on the comparison between the analytical solution and the published experimental work in the literature under static conditions. The uplift resistance is equal to the weight of the soil above the plate anchor and the shear resistance along the failure ruptures (e.g., White *et al*. 2008, Evans and Zhang 2019). The calculation of soil weight above the plate anchor is straightforward, however, an assumption might be necessary to calculate the shearing resistance along the failure rupture. The shearing resistance along the failure ruptures are assumed to be relying on the passive resistance (Meyerhof and Adams 1968, Murray an Geddes 1987, Geddes and Murray 1991) to resist the tension force arising from anchor pullout. Referring to White *et al.* (2008), the peak shear stress along the failure rupture can be obtained from the Mohr's circle shown in Fig. 6. During uplifting, the passive resistance is mobilized and outer circle in Fig. 6 represents the stress conditions at peak resistance. The bold arrow indicates, at certain depth, the shear stress would increase while the normal stress keeps constant. The shear stress along the failure rupture can be obtained from the geometry of the Mohr's circle in Fig. 6 as Eq. (44).

$$\tau = \gamma_{sub} z\left[\frac{K_p+1}{2}-\frac{K_p-1}{2}\cos(2\psi)\right]\tan\phi \tag{44}$$

where K_p is the passive earth pressure coefficient, ψ is the dilation angle, φ is the internal friction angle. The shearing force of the unit length applied on the right rupture is defined as Eq. (45).

$$T_+ = \int_0^{S_+} \tau ds = \int_0^H \frac{R_R}{\sqrt{R_R^2-\left(z+R_R\sin\alpha\right)^2}}\tau dz \tag{45}$$

The shearing force of the unit length applied on the left rupture is defined as Eq. (46).

$$T_- = \int_0^{S_-} \tau ds = \int_0^{H-\frac{L}{2}\sin\alpha} \frac{z^2}{R_L^2-z^2}\tau dz \tag{46}$$

The anchor holding resistance can be calculated as the summation of submerged soil weight and the shearing force on the ruptures as Eq. (47)

$$Q = W + T_+ + T_- \tag{47}$$

The breakout factor can therefore be calculated as Eq. (48).

$$N_\gamma = \frac{Q_s}{\gamma HL} \tag{48}$$

where N_γ is the static breakout factor, Q_s is the static holding resistance of the plate anchor.

Fig. 7 shows the comparison between the analytical solution in the static condition and results published in the literature. In general, the break-out factor N_γ varies linearly with the increase of embedment ratio, which is defined as the the ratio of embedment depth to anchor width. The

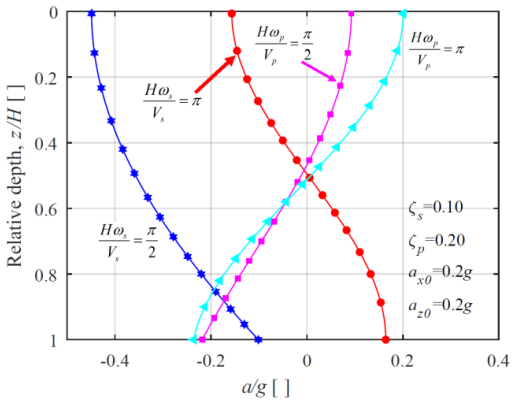

Fig. 8 Distribution of S-wave and P-wave accelerations

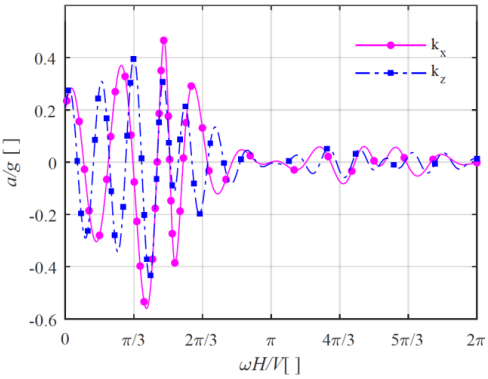

Fig. 9 Seismic coefficients as functions of normalized frequency at anchor depth *H*

Table 1 Parameters (baseline) used in the analytical calculation (e.g., Fang 1991, Rix *et al*. 2000)

Parameter	Values	Parameter	Values
G [ ]	1×10^8	λ [ ]	0.30
ζ_s [ ]	0.10	ζ_p [ ]	0.20
γ_{sub} [kN/m3]	11.7	γ [kN/m^3]	21.5
E_s [kPa]	5×10^4	g [m/s^2]	9.81
a_{x0} [ ]	0.2 g	a_{z0} [ ]	0.2 g
H_w/H	1.0		

results from the analytical solution are consistent with the results published in the literature. Due to the conservative assumptions made, the results reported by Merifield and Sloan (2006) and Dyson and Rognon (2014) are smaller than the present solution. Another reason lies that only the passive pressures are assumed on the failure ruptures without considering the friction shearing pressures. Current solution is most consistent with the upper-bound solution of Murray and Geddes (1987). Nonetheless, the breakout factor obtained from the present solution exhibits a rate of increase with the increasing embedment ratio that similar to the experimental results.

The acceleration distribution of the soil above the plate anchor is shown in Fig. 8. Fig. 8 shows an example of soil acceleration distributions for two different $\omega_s H/V_s$ and $\omega_p H/V_p$ values when the damping in *x* and *z* directions are 0.10 and 0.20, respectively. The magnitudes of the

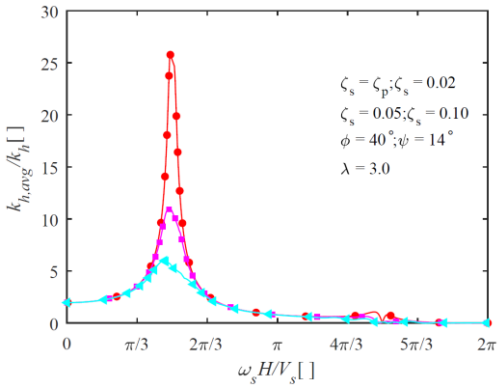

Fig. 10 The weighted average acceleration coefficients a s a function of normalized frequency of S-wave

horizontal and vertical acceleration at the lower edge of the plate anchor are denoted as a_{x0} and a_{z0}. It can be observed that at $\omega_s H/V_s=\pi$, the wedge is subjected to an acceleration in $+x$ direction while the upper half part is subjected to an acceleration in $-x$ direction. The maximum values at z/H=0, 1 are slightly smaller than the acceleration amplitude at the lower edge of the plate anchor. At $\omega_s H/V_s = \pi/2$, the whole wedge is subjected to an acceleration in $-x$ direction. The negative *x* acceleration will give an inertia force that resists the plate anchor from being pulling out as denoted in Fig. 2. At both $\omega_p H/V_p = \pi/2$ and $\omega_p H/V_p = \pi$, the upper half part of the wedge within the failure rupture meet with an acceleration in $+z$ direction while the lower half part of the wedge has an acceleration in $-x$ direction. The parameters used at the baseline are shown in Table 1.

Fig. 9 shows the seismic coefficients as functions of $\omega H/V$. Results show that k_x and k_z are larger for small angular frequencies. At lower $\omega H/V$, the k_x and k_z amplitudes increase with the normalized frequencies. There are amplification effects of accelerations at lower normalized frequency $\omega H/V$. The seismic coefficients for both shear and primary waves reach the maximum when the normalized frequency is around π/2, which corresponds to the normalized weighted average accelerations within the soil wedge shown in Fig. 10. The maximum magnitude of weighted average coefficients was found to increase followed by decreases after being reached the peak value at around $\omega H/V=\pi/2$, at which the shear wave reached the fundamental frequency. $k_{h,avg}/k_h$ is found to to decrease with the increasing of ζ_s.

3.2 Dynamic anchor holding coefficient

The dynamic anchor holding coefficient in this paper is defined as the total holding resistance over the soil weight right above the plate anchor as shown in Eq. (49).

$$N_{\gamma d}=\frac{T+Q_s+F_n-Q_u}{\gamma HL} \tag{49}$$

where *T* is the shear pressure on the failure rupture, Q_s is the static anchor holding resistance, F_n is the hydrodynamic pressure applied on the plate anchor, and Q_u is the inertia force applied on the plate anchor. For the latest-developed

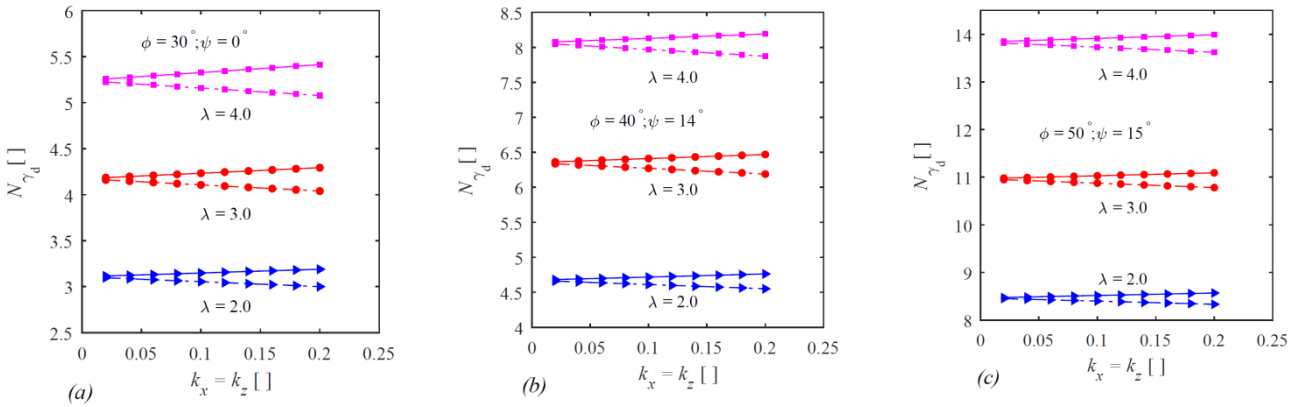

Fig. 11 Dynamic holding coefficients as functions of k_x, k_z for different embedment ratios (**note**: the solid lines denote the maximum value, the dash lines denote the minimum values), $\omega H/V=1/\pi$

PDA employed in the article, the amplification of the acceleration in the soil layer depends on the properties of soil layer, angular frequencies of shear, primary waves, embedment depth, time, and anchor inclinations. Soil internal friction, soil damping, anchor embedment depth, and anchor inclination are four different influential parameters on $N_{\gamma d}$ considering in the article.

3.2.1 Effects of internal friction

The dynamic holding coefficients $N_{\gamma d}$ have maximum and minimum values as the oscillating behavior of the waves, Fig. 11 shows the variation of the $N_{\gamma d}$ as functions of k_x and k_z for different embedment ratios λ with different soil properties. Soils shown in Fig. 11(a) have the weakest strength and Fig. 11(c) has the strongest strength. The larger the soil internal friction the larger the dynamic holding coefficient of the plate anchor. The solid line corresponds to the maximum dynamic holding coefficient and the dash line corresponds to the minimum values. The oscillation of the dynamic holding coefficient was essentially resulted from the oscillation of the inertia forces of the soil within the failure rupture and the hydrodynamic force applied on the plate anchor. Therefore, it can be stated that the minimum dynamic holding coefficients decrease with the k_x and k_z, which are related to the shear and primary wave velocities as shown in Eqs. (1) and (2) and Fig. 9. Once the minimum dynamic holding coefficient equal or smaller than zero, the soils will be liquefied.

3.2.2 Effects of damping ratio

Fig. 12 shows the dynamic holding coefficient $N_{\gamma d}$ as functions of the k_x and k_z values for different damping ratios at the same embedment ratio λ=3.0 and same relative water depth H_w/H. The damping ratio of the surface and primary wave are assumed to be the same, ζ_s=ζ_p. The internal friction angle φ=40° with dilation angle ψ = 14°. It is intuitive that $N_{\gamma d}$ increases or decreases the k_x and k_z values. And the larger the damping ratio, the smaller the oscillation. This can be explained that for smaller damping ratios, the soil acceleration further from the plate anchor will not decrease so much that the soil within the failure rupture will be excited. Soil wedge with larger acceleration will have the largest oscillation of inertia forces, which will result in the largest oscillation of $N_{\gamma d}$.

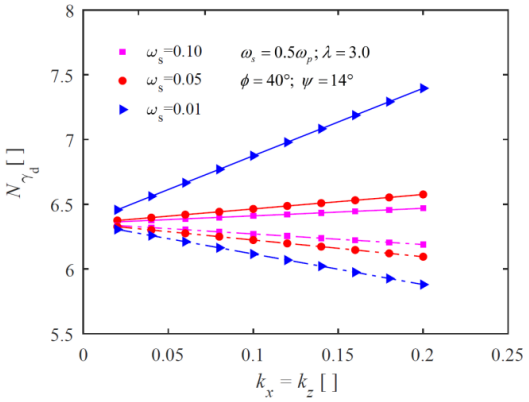

Fig. 12 Dynamic holding coefficients as functions of k_x, k_z for different damping ratios (λ=3.0) (note: the solid lines denote the maximum value, the dash lines denote the minimum values), $\omega H/V = 1/\pi$

3.2.3 Effects of anchor inclination

Fig. 13 shows the dynamic holding coefficient $N_{\gamma d}$ as functions of k_x and k_z for different anchor inclinations. The angular velocity meets $\omega_s = \omega_p$, the internal friction angle φ=40° with dilation angle ψ = 14°. Due to the oscillation of the wave loads, the largest and smallest values occur simultaneously. Therefore, the larger anchor inclination has the largest and smallest $N_{\gamma d}$. According to Figs. 2 and 8, the soil acceleration within the soil wedge in vertical direction has two different directions while in horizontal direction the acceleration within the soil wedge is mostly negative/positive. Eqs. (28) and (33) show that the inertia force of the soil wedge induces larger and smaller force on the plate anchor, respectively, when the anchor inclination is larger. Plate anchor with larger inclinations will have the largest oscillation under identical acceleration.

Fig. 14 examines the variation of the dynamic holding coefficient $N_{\gamma d}$ with time for different k_x and k_z values, at the given values of φ, ψ, λ and anchor inclination α. Referring to Fig. 5, the hydrodynamic pressure coefficient at specific anchor inclination is also constant. The dynamic holding coefficient varies with the inertia force applied on the plate anchor. Fig. 14 shows that $N_{\gamma d}$ oscillates around a constant value the static holding coefficient. The oscillation turns to be larger with the larger k_x and k_z values. $N_{\gamma d}$ at the smallest

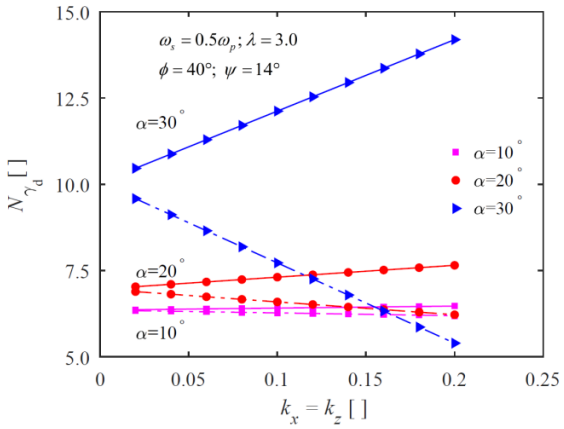

Fig. 13 Dynamic holding coefficients as functions of k_x, k_z for different anchor inclinations (λ = 3.0) (note: the solid lines denote the maximum value, the dash lines denote the minimum values), $\omega H/V = 1/\pi$

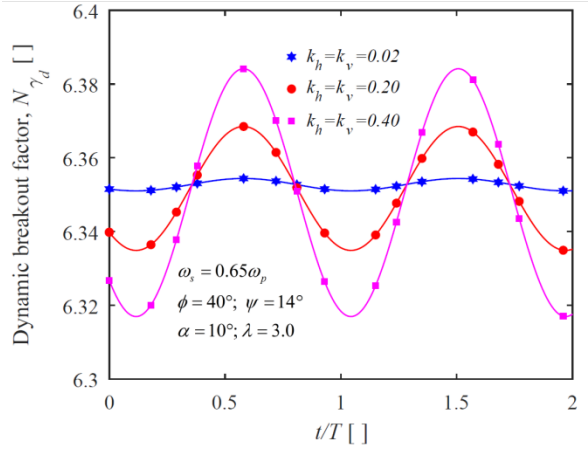

Fig. 14 Dynamic holding coefficients with t/T for different k_x, k_z

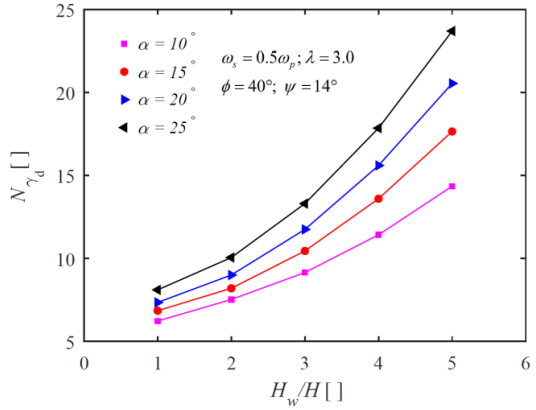

Fig. 15 Dynamic holding coefficients as a function of relative water depth for different anchor inclinations

k_x and k_z values have the smallest oscillations. $N_{\gamma d}$ have frequently maximum and minimum values with the time. k_x and k_z can influence the seismic holding capacities. The minimum $N_{\gamma d}$ values occur at t= 0.13s for all the selected cases.

Fig. 15 shows the dynamic anchor holding coefficients (minimum values) as a function of relative water depth H_w/H, where H_w is the water depth from anchor. Results show that the dynamic holding coefficients at smaller anchor inclinations are smaller than at the larger anchor inclinations. The larger the water depth, the larger dynamic holding coefficient of the inclined plate anchor. $N_{\gamma d}$ for anchor inclines at α=10° ranges from 6.23 to 14.35. $N_{\gamma d}$ for anchor inclines at α=25° ranges from 8.1 to 23.7. $N_{\gamma d}$ increases monotonically with the increasing relative depth. The changing rate is increasing with the increase of H_w/H. Apart from the static water pressure applied on the plate anchor which results in the linear relationship, the increase of changing rate is resulting from the hydrodynamic pressures applied. $N_{\gamma d}$ is found to be a convex function of relative water depth H_w/H.

4. Conclusions

The holding behaviors of the inclined plate anchor embedded into submerged coarse soils under seismic loading are presented in the paper. The upper-bound theorem of limit equilibrium analysis combined with the latest-introduced PDA are applied to investigate the influence of anchor inclinations on the seismic holding behaviors of the plate anchor. The exact potential flow theory is introduced to calculate the coefficient of hydrodynamic force applied on the inclined plate anchor. The current solutions consider the influence of both hydrodynamic pressures and soil inertia forces on the holding capacities of plate anchors with different inclinations. The influence of different factors such as the soil internal friction, damping ratio, and the anchor inclination are demonstrated in the paper. The conclusions can be drawn as follows:

- The static breakout factor N_γ obtained from the current analytical solution varies linearly with the increase of embedment ratio, which is consistent with the results published in the literature. The breakout factor obtained from the present solution exhibits a rate of increase with the increasing embedment ratio that similar to the experimental results.
- The seismic coefficients k_x and k_z are found to be larger for small angular frequencies. There are amplification effects of accelerations at lower $\omega H/V$. The seismic coefficients for both shear and primary waves reach the maximum when the normalized frequency is around $\pi/2$, which corresponds to the normalized weighted average accelerations within the soil wedge. The maximum magnitude of weighted average coefficients is found to increase and then decrease after reaching the peak value at around $\omega H/V = \pi/2$, at which the shear wave reaches the fundamental frequency. $k_{h,avg}/k_h$ is found to to decrease with the increasing of ζ_s.
- The dynamic holding coefficients as a function of k_x and k_z of the inclined plate anchor have the fluctuation behaviors, which results from the oscillation behaviors of the inertia forces of the assumed soils within the failure rupture. The oscillation turns to be larger with the larger k_x and k_z values. $N_{\gamma d}$ at smallest k_x and k_z values have smallest

oscillations. $N_{\gamma d}$ have frequently maximum and minimum values with the time. k_x and k_z can influence the seismic holding capacities. $N_{\gamma d}$ has been found to be a convex function of relative water H_w/H.

The analytical solution on the seismic holding capacity of inclined plate anchor embedded into coarse grained sandy soils was derived by incorporating pseudo-dynamic analysis, upper limit analysis, and exact potential flow theory. The dynamic holding coefficients were herein calculated with respect to the primary and surface wave properties. In engineering practice, the derived solution can be used to estimate the dynamic holding capacities of the inclined plate anchors and seismic/earthquake properties, such as primary and surface wave properties, and also the soil properties.

Acknowledgments

This research is partially supported by the National Key Research and Development Program of China (SN: 2019YFC1510801), National Natural Science Foundation of China (SN: 51979093), the Fundamental Research Funds for the Central Universities (2682021CX003 and 2682021ZTPY049). The author would also acknowledge the anonymous reviewers for their valuable comments to improve this work.

References

Bellezza, I. (2014), "A new pseudo-dynamic approach for seismic active soil thrust", *Geotech. Geolog. Eng.*, **32**(2), 561-576. https://doi.org/10.1007/s10706-014-9734-y.

Bellezza, I. (2015), "Seismic active earth pressure on walls using a new pseudo-dynamic approach", *Geotech. Geolog. Eng.*, **33**(4), 795-812. https://doi.org/10.1007/s10706-015-9860-1.

Bhattacharya, P. (2017), Pullout capacity of shallow inclined anchor in anisotropic and nonhomogeneous undrained clay. *Geomech. Eng.*, **13**(5), 825-844. https://doi.org/10.12989/gae.2017.13.5.825.

Bhattacharya, P. and Sahoo, S. (2017), "Uplift capacity of horizontal anchor plate embedded near to the cohesionless slope by limit analysis", *Geomech. Eng.*, **13**(4), 701-714. https://doi.org/10.12989/gae.2017.13.4.701.

Biradar, J., Banerjee, S., Shankar, R., Ghosh, P., Mukherjee, S., and Fatahi, B. (2019), "Response of square anchor plates embedded in reinforced soft clay subjected to cyclic loading", *Geomech. Eng.*, **17**(2), 165-173. https://doi.org/10.12989/gae.2019.17.2.165.

Chakraborty, D. and Choudhury, D. (2014), "Sliding stability of non-vertical waterfront retaining wall supporting inclined backfill subjected to pseudo-dynamic earthquake forces", *Appl. Ocean Res.*, 47, 174-182. https://doi.org/10.1016/j.apor.2014.05.004.

Choudhury, D. and Subba Rao, K.S. (2005), "Seismic uplift capacity of inclined strip anchors", *Can. Geotech. J.*, **42**(1), 263-271. https://doi.org/10.1139/t04-074.

Chwang, A.T. (1978), "Hydrodynamic pressures on sloping dams during earthquakes. Part 2. Exact theory", *J. Fluid Mech.*, **87**(2), 343-348. https://doi.org/10.1017/S0022112078001640.

Chwang, A.T. and Housner, G.W. (1978), "Hydrodynamic pressures on sloping dams during earthquakes. Part 1. Momentum method", *J. Fluid Mech.*, **87**(2), 335-341. https://doi.org/10.1017/S0022112078001639.

Dickin, E.A. (1988), "Uplift behavior of horizontal anchor plates in sand", *J. Geotech. Eng.*, **114**(11), 1300-1317. https://doi.org/10.1061/(ASCE)0733-9410(1988)114:11(1300).

Dyson, A.S. and Rognon, P.G. (2014), "Pull-out capacity of tree root inspired anchors in shallow granular soils", *Géotechnique Lett.*, **4**(4), 301-305. https://doi.org/10.1680/geolett.14.00061.

Evans, T.M. and Zhang, N. (2019). "Three-dimensional simulations of plate anchor pullout in granular materials", *Int. J. Geomech.*, **19**(4), 04019004. https://doi.org/10.1061/(ASCE)GM.1943-5622.0001367.

Fang, H.Y. (1991), *Foundation Engineering Handbook*. Chapman & Hall, New York, NY, USA

Ganesh, R., Khuntia, S. and Sahoo, J.P. (2018), "Seismic uplift capacity of shallow strip anchors: A new pseudo-dynamic upper bound limit analysis". *Soil Dyn. Earthq. Eng.*, **109**, 69-75. https://doi.org/10.1016/j.soildyn.2018.03.004.

Gaudin, C., Tham, K.H. and Ouahsine, S. (2008), "Plate anchor failure mechanism during keying process", *Proceedings of the 18th International Offshore and Polar Engineering Conference*. International Society of Offshore and Polar Engineers. Vancouver, July.

Geddes, J.D. and Murray, E.J. (1991), "Passive inclined anchorages in sand", *J. Geotech. Eng.*, **117**(5), 810-814. https://doi.org/10.1061/(ASCE)0733-9410(1991)117:5(810).

Ghosh, P. (2009), "Seismic vertical uplift capacity of horizontal strip anchors using pseudo-dynamic approach", *Comput. Geotech.*, **36**(1-2), 342-351. https://doi.org/10.1016/j.compgeo.2008.01.002.

Ghosh, P. (2010), "Seismic uplift capacity of inclined strip anchors in sand using upper bound limit analysis", *Geomech. Geoeng.*, **5**(4), 267-275. https://doi.org/10.1080/17486025.2010.492242.

Hardin, B.O. (1965), "The nature of damping in sands", *J. Soil Mech. Found. Div.*, **91**(1), 63-67.

Harvey, R.C. and Burley, E. (1973), "Behavior of shallow inclined anchorages in cohesionless sand", *Ground Eng.*, **6**(5).

Hossain, T. and Rognon, P. (2020), "Mobility in immersed granular materials upon cyclic loading", *Phys. Review E*, **102**(2), 022904. https://doi.org/10.1103/PhysRevE.102.022904.

Hu, S., Zhao, L., Tan, Y., Yang, F., Wang, Z. and Zhao, Z. (2021), "Variation analysis of uplift bearing characteristics of strip anchor plate in nonhomogeneous materials", *Int. J. Geomech.*, 21(4), 04021037. https://doi.org/10.1061/(ASCE)GM.1943-5622.0001974.

Ilamparuthi, K. and Muthukrishnaiah, K. (1999), "Anchors in sand bed: delineation of rupture surface", *Ocean Eng.*, **26**(12), 1249-1273. https://doi.org/10.1016/S0029-8018(98)00034-1.

Kramer, S.L. (1996), *Geotechnical Earthquake Engineering*. Prentice-Hall, New Jersey, USA.

Kumar, J. (2001), "Seismic vertical uplift capacity of strip anchors", *Geotechnique*, **51**(3), 275-279. https://doi.org/10.1680/geot.2001.51.3.275.

Kumar, J. and Kouzer, K.M. (2008), "Vertical uplift capacity of horizontal anchors using upper bound limit analysis and finite elements", *Can. Geotech. J.*, **45**(5), 698-704. https://doi.org/10.1139/T08-005.

Liang, W., Zhao, J., Wu, H. and Soga, K. (2021), "Multiscale modeling of anchor pullout in sand", *J. Geotech. Geoenviron. Eng.*, **147**(9), 04021091. https://doi.org/10.1061/(ASCE)GT.1943-5606.0000633

Liu, J., Liu, M. and Zhu, Z. (2012), "Sand deformation around an uplift plate anchor", *J. Geotech. Geoenviron. Eng.*, **138**(6), 728-737. https://doi.org/10.1061/(ASCE)GT.1943-5606.0000633.

Matsuzawa, H., Ishibashi, I. and Kawamura, M. (1985), "Dynamic soil and water pressures of submerged soils", *J. Geotech. Eng.*, **111**(10), 1161-1176. https://doi.org/10.1061/(ASCE)0733-

9410(1985)111:10(1161).

Merifield, R.S., Lyamin, A.V., Sloan, S.W. and Yu, H.S. (2003), "Three-dimensional lower bound solutions for stability of plate anchors in clay", *J. Geotech. Geoenviron. Eng.*, **129**(3), 243-253. https://doi.org/10.1061/(ASCE)1090-0241(2003)129:3(243).

Merifield, R.S. and Sloan, S.W. (2006), "The ultimate pullout capacity of anchors in frictional soils", *Can. Geotech. J.*, **43**(8), 852-868. https://doi.org/10.1139/t06-052.

Meyerhof, G.G. and Adams, J.I. (1968), "The ultimate uplift capacity of foundations", *Can. Geotech. J.*, **5**(4), 225-244. https://doi.org/10.1139/t68-024.

Mononobe, N. (1929), "On determination of earth pressure during earthquake", *Proceedings of the World Engineering Congress*.

Murray, E.J. and Geddes, J.D. (1987), "Uplift of anchor plates in sand", *J. Geotech. Eng.*, **113**(3), 202-215. https://doi.org/10.1061/(ASCE)0733-9410(1987)113:3(202).

O'Loughlin, C.D. and Barron, B. (2012), "Capacity and keying response of plate anchors in sand", *Proceedings of the Offshore Site Investigation and Geotechnics: Integrated Technologies-Present and Future*. London, September.

O'Loughlin, C.D., Lowmass, A., Gaudin, C. and Randolph, M.F. (2006), "Physical modelling to assess keying characteristics of plate anchors", *Proceedings of the 6th international conference on physical modelling in geotechnics*, Hong Kong, August.

Pain, A., Choudhury, D. and Bhattacharyya, S.K. (2016), "Seismic uplift capacity of horizontal strip anchors using a modified pseudodynamic approach", *Int. J. Geomech.*, **16**(1), 04015025. https://doi.org/10.1061/(ASCE)GM.1943-5622.0000471.

Rajesh, B.G. and Choudhury, D. (2017), "Seismic passive earth resistance in submerged soils using modified pseudo-dynamic method with curved rupture surface", *Mar. Georesour. Geotec.*, **35**(7), 930-938. https://doi.org/10.1080/1064119X.2016.1260077.

Randolph, M. and Gourvenec, S. (2011), *Offshore Geotechnical Engineering*. CRC press, New York, USA

Rangari, S.M., Choudhury, D. and Dewaikar, D.M. (2013), "Seismic uplift capacity of shallow horizontal strip anchor under oblique load using pseudo-dynamic approach", *Soils Foundations*, **53**(5), 692-707. https://doi.org/10.1016/j.sandf.2013.08.007.

Rix, G.J., Lai, C.G. and Spang Jr, A.W. (2000), "In situ measurement of damping ratio using surface waves", *J. Geotech. Geoenviron. Eng.*, **126**(5), 472-480. https://doi.org/10.1061/(ASCE)1090-0241(2000)126:5(472).

Rowe, R.K. and Davis, E.H. (1982). "The behaviour of anchor plates in sand", *Géotechnique*, **32**(1), 25-41. https://doi.org/10.1680/geot.1982.32.1.25.

Song, Z., Hu, Y., O'Loughlin, C. and Randolph, M.F. (2009), "Loss in anchor embedment during plate anchor keying in clay", *J. Geotech. Geoenviron. Eng.*, **135**(10), 1475-1485. https://doi.org/10.1061/(ASCE)GT.1943-5606.0000098.

Steedman, R.S. and Zeng, X. (1990), "The influence of phase on the calculation of pseudo-static earth pressure on a retaining wall", *Géotechnique*, **40**(1), 103-112. https://doi.org/10.1680/geot.1990.40.1.103.

White, D.J., Cheuk, C.Y. and Bolton, M.D. (2008), "The uplift resistance of pipes and plate anchors buried in sand", *Géotechnique*, **58**(10), 771-779. https://doi.org/10.1680/geot.2008.3692.

Yu, L., Liu, J., Kong, X.J. and Hu, Y. (2009), "Three-dimensional numerical analysis of the keying of vertically installed plate anchors in clay", *Comput. Geotech.*, **36**(4), 558-567. https://doi.org/10.1016/j.compgeo.2008.10.008.

Yuan, C., Peng, S., Zhang, Z. and Liu, Z. (2006), "Seismic wave propagating in Kelvin-Voigt homogeneous visco-elastic media", *Sci. China Series D*, **49**(2), 147-153. https://doi.org/10.1007/s11430-004-5138-9.

Zangar, C.N. (1953), "Hydrodynamic pressures on dams due to horizontal earthquakes", *Proceedings of the Soc. for Experimental Stress Analysis*, Cambridge, UK.

Zhang, N. (2018), "Numerical simulations and microscale analyses of offshore anchor-granular material systems", Ph.D. dissertation, Oregon State University, Corvallis.

Zhang, N., Evans, T.M., Zhao, S., Du, Y. and Zhang, L. (2020), "Discrete element method simulations of offshore plate anchor keying behavior in granular soils", *Mar. Georesour. Geotec.*, **38**(6), 716-729. https://doi.org/10.1080/1064119X.2019.1614705.

CC